

We are IntechOpen, the world's leading publisher of Open Access books Built by scientists, for scientists

6,900

Open access books available

186,000

International authors and editors

200M

Downloads

Our authors are among the

154

Countries delivered to

TOP 1%

most cited scientists

12.2%

Contributors from top 500 universities



WEB OF SCIENCE™

Selection of our books indexed in the Book Citation Index
in Web of Science™ Core Collection (BKCI)

Interested in publishing with us?
Contact book.department@intechopen.com

Numbers displayed above are based on latest data collected.
For more information visit www.intechopen.com



Maximal Operational Workspace of Parallel Manipulators

E. Macho, O. Altuzarra and A. Hernandez
University of Basque Country.
Faculty of Engineering in Bilbao.
Department of Mechanical Engineering
Spain

Nomenclature

Symbol	Meaning
MP	Mobile platform
KC	Kinematic chain(s)
TCP	Tool center point
DOF	Degree(s) of freedom
IKP	Inverse kinematic problem
DKP	Direct kinematic problem
$ J_{IKP} $	Inverse Jacobian
$ J_{DKP} $	Direct Jacobian

The term *kinematic chain* is used in the sense of limb, or *leg*, of the parallel manipulator.

1. Introduction

Parallel manipulators are an interesting alternative to serial robots given the important mechanical and kinematic advantages offered. Nevertheless, they often present more complex and smaller workspaces with internal singularities (Altuzarra et al., 2004; Gosselin & Angeles, 1990). Thus, the workspace size, shape and quality are considered some of the main design criteria of these robots (Merlet et al., 1998).

These robots often present multiple solutions for both the DKP and the IKP . The workspace singularity-free region where the manipulator is initially configured, i.e., the set of postures that a manipulator can reach in the same direct and inverse configuration, has been traditionally considered its operational workspace. This is due to the fact that it is widely extended the idea that to perform a transition between different kinematic solutions, the robot must cross a singular position where the control is lost, and that must be avoided (Hunt & Primrose, 1993). This idea leads to very limited operational workspaces.

In this chapter, a general methodology for obtaining the maximal operational workspace where a parallel manipulator can move in a controllable way will be presented. The basis for enlarging the operational workspace consists in superimposing all the singularity-free regions of the workspace associated with the same assembly mode for all different robot work-

ing modes. This work is the generalization of the methodology developed in (Macho et al., 2008b) for a planar two-*DOF* parallel manipulator, the 5R robot.

According to this, the first step is to develop a methodology capable of obtaining the complete workspace, i.e., the entire set of positions that a point of interest of the *MP*, the *TCP*, can reach. There are three main families of methodologies used to obtain the workspace of a manipulator, namely, discretization methods (Dash et al., 2002; Masory & Wang, 1995), geometrical methods (Bonev & Ryu, 1999; Gosselin, 1990) and analytical methods (Agrawal, 1991; Jo & Haug, 1998). In this case, the general purpose hybrid analytical-discrete procedure applicable to fully-parallel manipulators described in (Macho et al., 2009) will be used. Secondly, a complete singularity analysis must be done to carry out an efficient path planning. Singularity maps are traced for target manipulators making a kinematic analysis of the positions comprising the calculated workspace. To do this a systematic method to obtain the corresponding Jacobian matrices is introduced. This methodology is based on the mathematical disassembling of the manipulator into a *MP* and a set of serial *KC*.

Two main types of kinematic singularities are obtained. On the one hand, the *IKP* singularities which separate the different working modes of the robot and define the workspace boundaries, since they occur whenever a *KC* reaches an extreme position. At these postures a dependence relation among the output velocities appears, so the output capabilities of the *MP* are restricted, which is equivalent to an instantaneous reduction in the number of *DOF*. However, the manipulator can reach *IKP* singularities without compromising its controllability. On the other hand, *DKP* singularities, which are different for each working mode, occur inside the workspace and separate the different assembly modes of the robot (Li et al., 2007). At direct kinematic singularities a dependence relation among the input velocities occurs, which implies the robot becoming uncontrollable. The result of the whole process developed is the computation of all singularity-free workspace regions where the robot is fully controllable, associated with certain working and assembly modes.

This research shows the possibility of enlarging the operational workspace joining the different working modes through the *IKP* singularities, maintaining at all times the same assembly mode, that is, avoiding reaching a *DKP* singularity. Thus, the maximal operational workspace associated with a certain assembly mode of the robot is the union of the different singularity-free regions associated with that assembly mode from all working modes. In order to make a path planning inside this enlarged operational workspace, the strategies to identify the *IKP* singularities which connect the different regions joined will be provided. To illustrate all these general purpose procedures and strategies, an example of application will be proposed. A spatial complex parallel manipulator is the most appropriate candidate to show the potentiality, effectiveness and interest of this methodology.

The different solutions of the *IKP* of a parallel manipulator are known as working modes. In the same way, the different solutions of the *DKP* have been traditionally known as assembly modes. Nevertheless, in this chapter the concept of assembly mode will have a different meaning. It is well known that some parallel manipulators are able of moving from one *DKP* solution to another in a fully controlled way, i.e., without crossing any *DKP* singularity. These are the so-called cuspidal robots (Innocenti & Parenti-Castelli, 1992; McAree & Daniel, 1999). The notion of assembly mode as *DKP* solution is confusing in cuspidal robots, because different *DKP* solutions can be joined without losing control and in fact, joined solutions are geometrically indistinguishable. In this work, those *DKP* solutions between which the manipulator can alternate without crossing a *DKP* singularity will not be considered different assembly modes. Assembly modes will be considered those kinematic configurations sepa-

rated by DKP singularities, always characterized by different signs of $|J_{DKP}|$, or which require the physical disassembling of the manipulator to be reached (Macho et al., 2008a).

2. A case study of translational manipulator

The manipulator shown in Fig. 1 is a three- DOF spatial parallel robot. It has two similar KC actuated each one by means of a prismatic joint along a fixed sliding direction and a third KC actuated by a fixed revolute joint. This is a fully-parallel manipulator since it has one actuated joint per KC . In fully-parallel manipulators the number of KC and, therefore, the number of input variables coincides also the number of DOF (output variables). The kinematic structure of these three KC , containing articulated parallelograms, causes a manipulator having just three translational DOF . These are known as *Delta-like KC*. There are several well known mechanisms based on this kind of kinematic structure, like the DELTA Robot. The singular configurations of these types of robots is analyzed in (Gregorio, 2004; Lopez et al., 2005) and the workspace in (Laribi et al., 2007; Liu et al., 2004). This example is suitable to illustrate the operational workspace enlargement general strategies due to the complexity of its singularity loci. Probably, the robot in Fig. 1 is not the most adequate at a practical level, but it has been found interesting for research purposes. Motion limitations in the kinematic joints will not be considered. Neither interferences or collisions among elements.

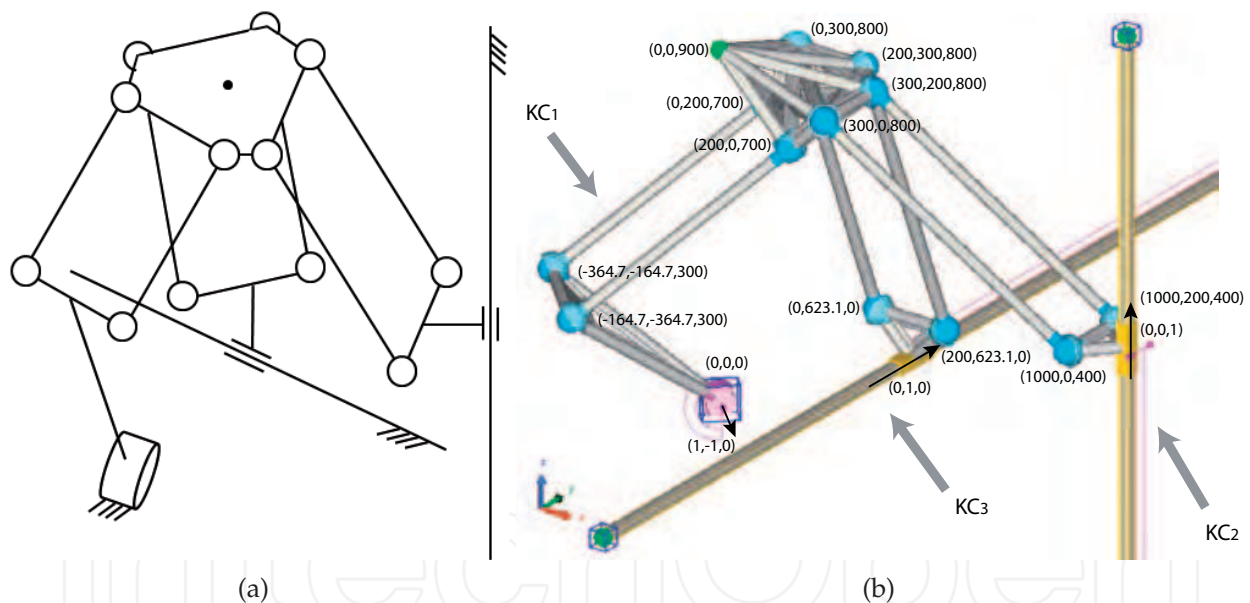


Fig. 1. *Delta-like* translational manipulator

An equivalent mechanism which will provide the same workspace and the same singularity loci will be analyzed. This is the manipulator shown in Fig. 3. Each KC of the original mechanism in Fig. 1 is split in two, breaking the parallelogram. The KC actuated by the revolute joint (KC_1 in Fig. 1) is split in two \underline{RSS} KC , like shown in Fig. 2-(a), and each of the two KC actuated by a prismatic joint (KC_2 and KC_3 in Fig. 1) split in two \underline{PSS} KC , Fig. 2-(b). The resulting fully-parallel manipulator has six-uncoupled- DOF . The MP can change its position and also spatial orientation. The kinematics of manipulators in Fig. 1 and Fig. 3 will be similar if the resulting couples of KC (Fig. 2) are actuated imposing for both KC the same input variable. Therefore the workspace and singularity loci of the manipulator in Fig.

1 can be obtained computing the constant orientation workspace of the manipulator in Fig. 3. The reason for analyzing the auxiliary manipulator instead of the real one is because it will be used a method capable of solving the kinematics of manipulators with \underline{RSS} and \underline{RSS} KC.

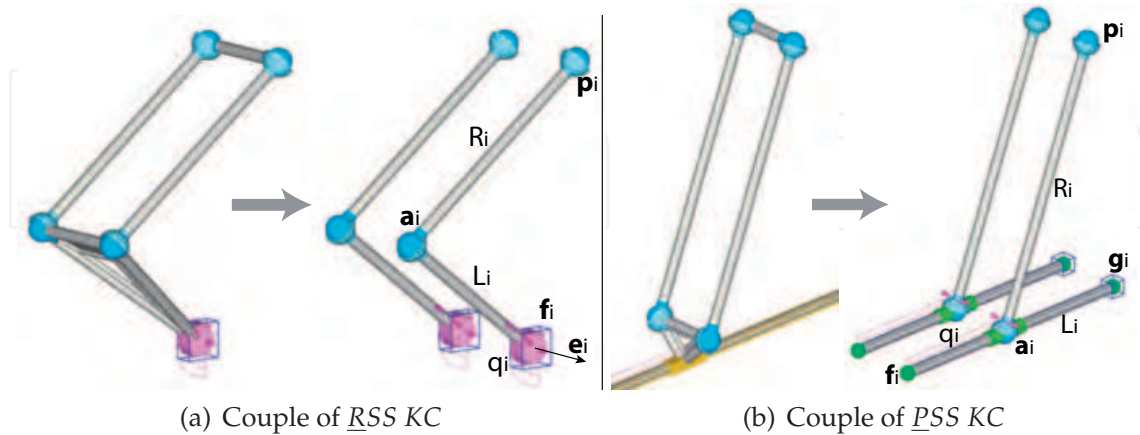


Fig. 2. Auxiliary equivalent KC

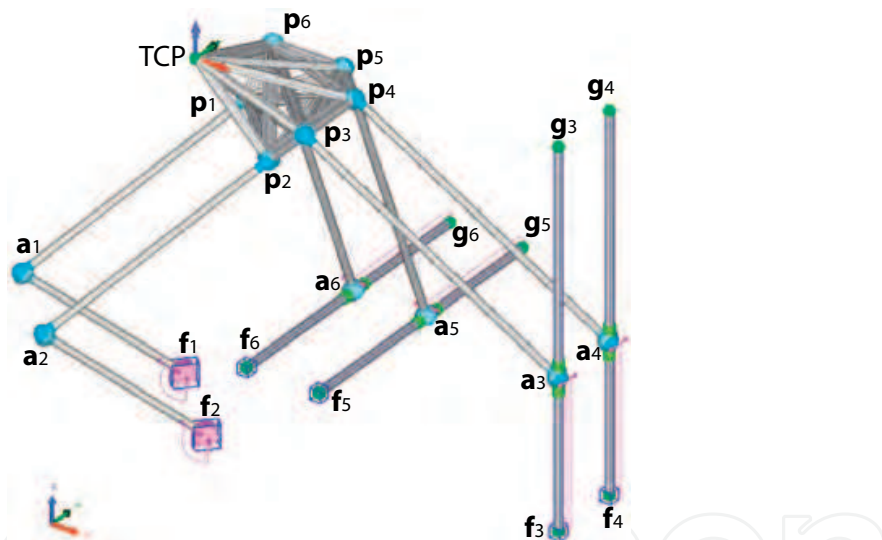


Fig. 3. Auxiliary equivalent 4- \underline{PSS} -2- \underline{RSS} manipulator

In the original manipulator each of the three KC has two *IKP* configurations. Thus, the whole manipulator has a total of eight (2^3) working modes. In the auxiliary manipulator, each of the six equivalent KC as also two *IKP* configurations. Thus, the auxiliary manipulator has a total of sixty four (2^6) working modes, but just the eight coincident with those of the original manipulator will be considered. These are shown in Fig. 4. The nomenclature used is $WM_{c_1c_2c_3}$, where c_1 , c_2 and c_3 stand for configuration of KC_1 , KC_2 and KC_3 respectively, being either p (positive) or n (negative). For the analyzed manipulator, when the *IKP* has solution, each KC can have two different configurations. Mathematically those come from a quadratic equation where the two distinct solutions correspond to the use of a positive or negative sign.

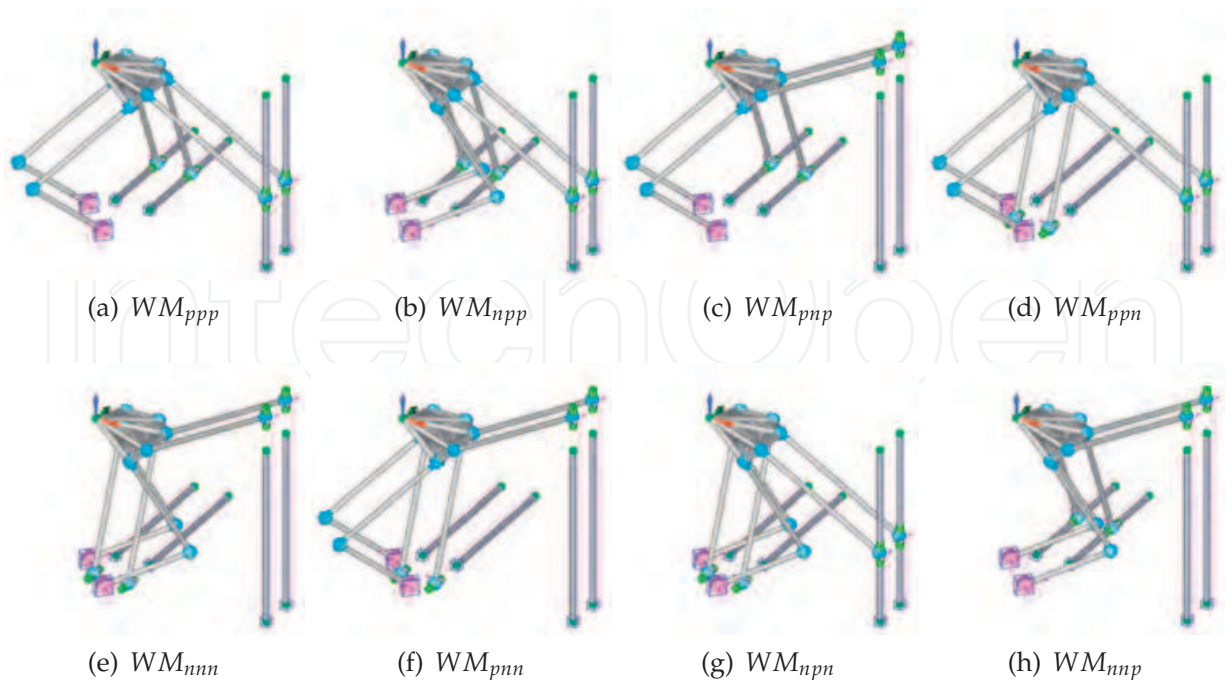


Fig. 4. Working modes considered in the auxiliary manipulator

3. Workspace computation

In order to compute the workspace, as well as to make the kinematic analysis to determine the singularity surfaces crossing and dividing the workspace into the singularity-free regions, a mathematical model of the robotic device must be done. In parallel manipulators, a *MP* is attached to a fixed frame through a set of *KC*. Therefore, the mathematical model developed to compute the workspace and the singularities consists in first separating the *MP* from each *CK*. The following notion for these basic entities of the model will be used.

The *MP* is a rigid body located in a reference frame $(O, \mathbf{i}, \mathbf{j}, \mathbf{k})$, by virtue of a moving frame $(TCP, \mathbf{u}, \mathbf{v}, \mathbf{w})$ attached to it, as shown in Fig. 5. The coordinates of the origin, position of the *TCP*, are the translational output variables (X, Y, Z) . In a six-*DOF* manipulator, the spatial orientation of such a system is given by the rotational output variables of the *MP*, the three Euler angles (φ, θ, ψ) , in their *ZYZ* version. In this moving frame, the position of the nodes where *KC* are attached to the *MP* are given by constant coordinates (x_{pi}, y_{pi}, z_{pi}) .

A *KC* can be considered as an open limb with a large variety of topologies. In this example only *RSS* and *PSS* cases, shown in Fig. 2, appear. In fully-parallel manipulators, the number of *KC* is equal to the number of *DOF* and thus, each *KC* has a single actuated joint. Actuated joints are underlined and define input variables, denoted as q_i . Nodes where *KC* are attached to the *MP* are denoted by $\mathbf{p}_i = [X_{pi}, Y_{pi}, Z_{pi}]$. Nodes fixed to the base frame are $\mathbf{f}_i = [X_{fi}, Y_{fi}, Z_{fi}]$. For the *PSS* *KC*, to define the fixed sliding direction two nodes are used, \mathbf{f}_i and $\mathbf{g}_i = [X_{gi}, Y_{gi}, Z_{gi}]$. Finally, intermediate nodes, those whose position is different according to the *IKP* configuration, are given by $\mathbf{a}_i = [X_{ai}, Y_{ai}, Z_{ai}]$. Further constant parameters are also considered, e.g. magnitudes like $R_i, L_i...$

The workspace is computed using a hybrid discrete-analytical procedure. The complete workspace of the manipulator depicted in Fig. 3 is a six-dimensional continuum entity. The method presented in (Macho et al., 2009) makes an approximation of the actual continuum by

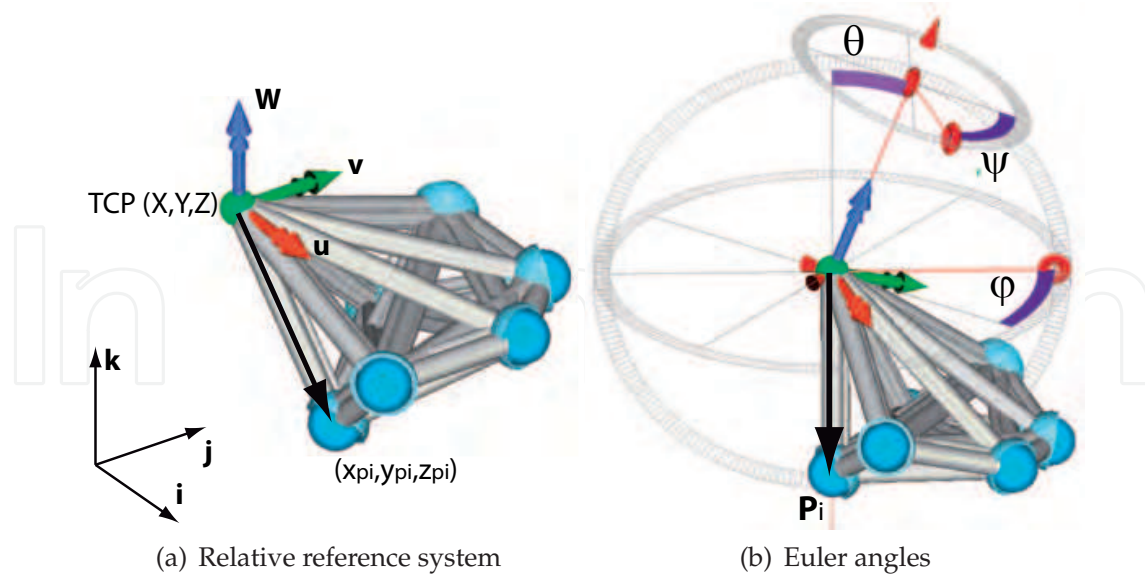


Fig. 5. Output variables defining the pose of the *MP*

a discretization of this real domain. On each point of such a discretized workspace, however, all calculations are done analytically.

The grid of discrete positions can be configured to the desired number of dimensions. Each dimension of such a grid contains an output variable to be incremented. All the remaining output variables, those not considered in the grid, will maintain a constant value. For example in Fig. 3, the case under analysis, a three-dimensional grid will be configured. Each dimension will increment one of the translation output variables (X, Y, Z). This way, since all the rotational output variables (φ, θ, ψ) will maintain a constant value, the constant orientation workspace of the manipulator will be computed. The constant orientation workspace is a three-dimensional subspace of the complete six-dimensional workspace. But the reader must remember that the constant orientation workspace of the manipulator in Fig. 3 is the total workspace of the original manipulator depicted in Fig. 1.

The most efficient method for providing the discrete candidate poses to the workspace is based on the propagation of a wave front. Starting from the pose where the manipulator is initially assembled, since this pose evidently belongs to the workspace. New poses, potentially belonging to the workspace, will be generated in the surroundings of those which have already provided satisfactory results, as shown schematically in Fig. 6 for a two-dimensional case.

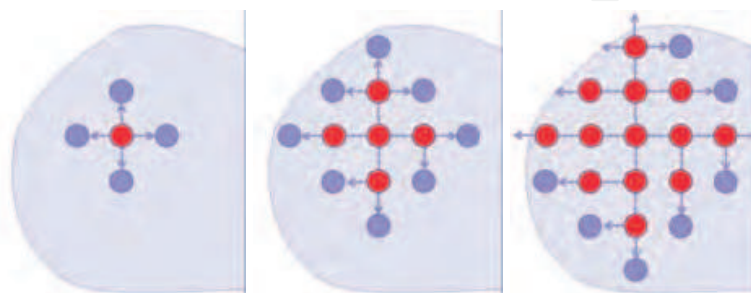


Fig. 6. Schematic advance of a wave front

The increment step for each *DOF* of the *MP* considered in the grid has to be defined. New candidate poses will be generated by incrementing each of the output variables considered, separately and in both senses, increasing and decreasing. This provides propagating capability in all directions of the domain comprising the subset of the workspace being computed. Each candidate pose will be tested to know if it has to be added to the workspace or not. The final result will be the workspace connected to the starting pose.

To check if a candidate pose belongs or not to the workspace, a verification of the *IKP* solution existence is performed. As this has to be done on a large number of poses, the most efficient method, the analytical one, has been chosen. Once the *MP* has been positioned according to the values of the output variables given by a point on the discrete grid, such a pose belongs to the workspace if and only if all *KC* can be physically assembled. As the *IKP* for parallel robots is an uncoupled problem, each *CK* is now considered as an independent sub-mechanism. The whole manipulator can be assembled when all *KC* can be assembled individually.

Once the *MP* is positioned in a specific location, the coordinates of the nodes at the end-joints \mathbf{p}_i of each *KC* are defined. These positions and the *KC* dimensions are the data necessary to first check the existence of solution, and afterwards solve the *IKP*. As each *KC* is treated separately, next will be shown the algorithms applied to the two types of *KC* involved in the present manipulator, shown in Fig. 2.

- *PSS KC*: node \mathbf{a}_i is located at the two possible intersections of a sphere centered at \mathbf{p}_i , with radius R_i and a line between points \mathbf{f}_i and \mathbf{g}_i .
- *RSS KC*: node \mathbf{a}_i is located at the two possible intersections of a sphere centered at \mathbf{p}_i , with radius R_i and a circumference centered at \mathbf{f}_i , with axis \mathbf{e}_i and radius L_i .

In Fig. 7-(a) is shown the result of this computation.

4. Singularity analysis

4.1 Velocity problem

The previous result still has not all the information required to plan a safe motion. Singularity maps will be traced by carrying out a kinematic analysis of the positions obtained in the previous step. A systematic method to obtain the corresponding *DKP* and *IKP* Jacobian matrices has been developed. These matrices come from performing the derivatives with respect to time on the position equations. In fully-parallel manipulators, since the number of *DOF* coincides with the number of *KC*, a position equation will be posed for each *KC*.

This position equation is specific for each *KC* topology and it is called characteristic equation. It is posed always in the same systematic way, in function of three types of parameters, the coordinates of the node attached to the *MP* (X_{pi}, Y_{pi}, Z_{pi}) the input variable or actuator position (q_i) and the dimensional parameters, (R_i, L_i, \dots), including here also the coordinates of fixed nodes ($X_{fi}, Y_{fi}, Z_{fi}, \dots$). This way, each *KC* is initially considered an independent sub-mechanism with its own position equation. In the case of *RSS* and *PSS KC*, the characteristic equation, $f_i = 0$, is given by Equation 1. The difference between both types of *KC* lies in the expressions $\mathbf{a}_i(q_i)$, the coordinates of the node \mathbf{a}_i in function of the input variable.

$$f_i = (X_{pi} - X_{ai}(q_i))^2 + (Y_{pi} - Y_{ai}(q_i))^2 + (Z_{pi} - Z_{ai}(q_i))^2 - R_i^2 = 0 \quad (1)$$

Next step consists in performing the assembly of these equations to the output variables, which is the application of the physical assembly of *KC* to the *MP*. This mathematical assembly is performed by substituting in the characteristic equations f_i , the end joint coordinates

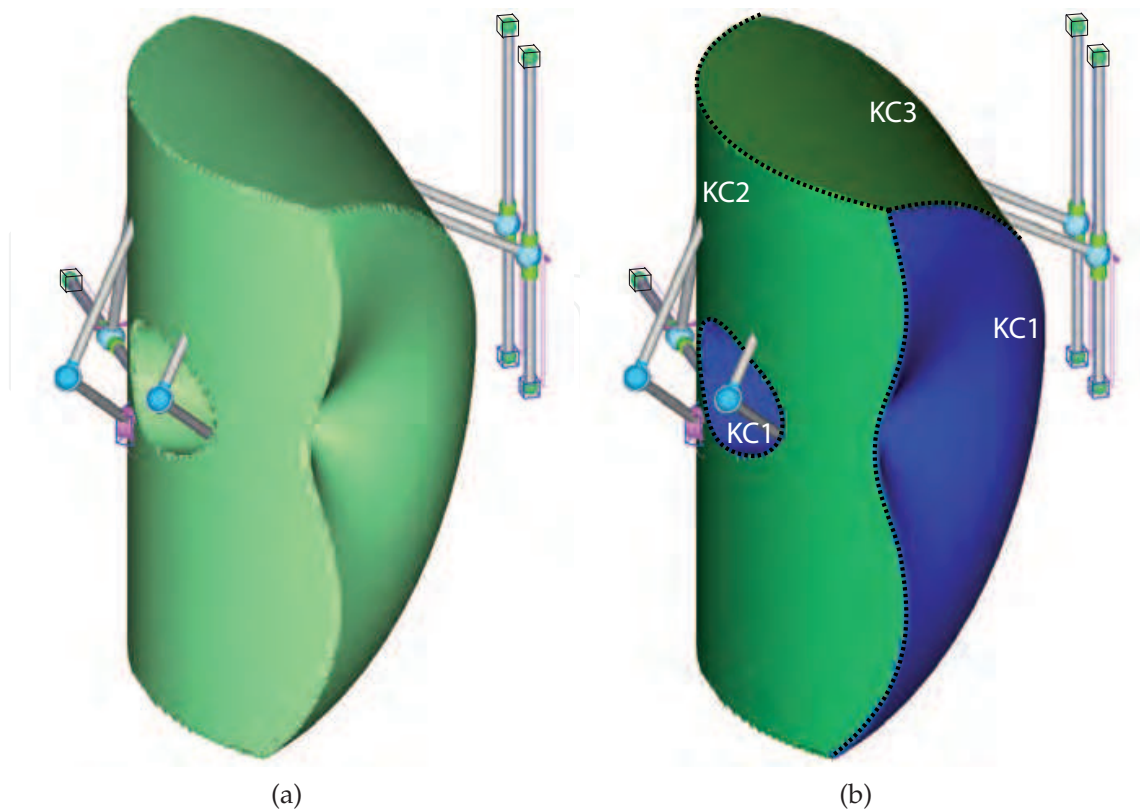


Fig. 7. Workspace

(X_{pi}, Y_{pi}, Z_{pi}) , as functions of the output variables $\mathbf{X} = (X, y, Z, \varphi, \theta, \psi)$. Taking into account Fig. 5, these functions are given in Equation 2.

$$\begin{pmatrix} X_{pi} \\ Y_{pi} \\ Z_{pi} \end{pmatrix} = \begin{pmatrix} X \\ Y \\ Z \end{pmatrix} + \begin{bmatrix} c\varphi & -s\varphi & 0 \\ s\varphi & c\varphi & 0 \\ 0 & 0 & 1 \end{bmatrix} \begin{bmatrix} c\theta & 0 & s\theta \\ 0 & 1 & 0 \\ -s\theta & 0 & c\theta \end{bmatrix} \begin{bmatrix} c\psi & -s\psi & 0 \\ s\psi & c\psi & 0 \\ 0 & 0 & 1 \end{bmatrix} \begin{pmatrix} x_{pi} \\ y_{pi} \\ z_{pi} \end{pmatrix} \quad (2)$$

The resulting system of six non-linear equations is dependent on the six output variables X_i and the six input variables q_i . By differentiating this system with respect to time, the velocity equations are obtained. This linear system of equations can be expressed in the matrix form given by Equation 3, being those matrices the *DKP* and *IKP* Jacobian (\mathbf{J}_{DKP} and \mathbf{J}_{IKP} respectively).

$$\begin{bmatrix} \frac{\partial f}{\partial \mathbf{X}} \end{bmatrix} \dot{\mathbf{X}} = \begin{bmatrix} -\frac{\partial f}{\partial \mathbf{q}} \end{bmatrix} \dot{\mathbf{q}} \quad (3)$$

4.2 DKP Jacobian matrix

To pose \mathbf{J}_{DKP} , the derivatives with respect to all output variables must be considered, independently from those chosen to compute a subset of the complete workspace. Since the actual auxiliary manipulator is a six *DOF* robot, the derivatives of the position equations with respect to the three translational output variables (X, Y, Z) and with respect to the three angular

ones (φ, θ, ψ) have to be performed, although just the translational variables have been incremented in the discrete grid to compute the constant orientation workspace.

Each element a_{ij} of \mathbf{J}_{DKP} in Equation 3 is given by:

$$a_{ij} = \frac{\partial f_i}{\partial X_j} = \frac{\partial f_i}{\partial X_{pi}} \frac{\partial X_{pi}}{\partial X_j} + \frac{\partial f_i}{\partial Y_{pi}} \frac{\partial Y_{pi}}{\partial X_j} + \frac{\partial f_i}{\partial Z_{pi}} \frac{\partial Z_{pi}}{\partial X_j} \quad (4)$$

On the one hand appear the partial derivatives of the position equations f_i with respect to the end-joint coordinates (X_{pi}, Y_{pi}, Z_{pi}), which can be directly obtained from Equation 1. On the other hand, the partial derivatives of such coordinates with respect to the output variables X_j are independent from f_i and they can be obtained from Equation 2. For translational output variables (X, Y, Z) those expressions are immediate:

$$\frac{\partial X_{pi}}{\partial X} = 1 \quad \frac{\partial X_{pi}}{\partial Y} = 0 \quad \frac{\partial X_{pi}}{\partial Z} = 0 \quad (5)$$

$$\frac{\partial Y_{pi}}{\partial X} = 0 \quad \frac{\partial Y_{pi}}{\partial Y} = 1 \quad \frac{\partial Y_{pi}}{\partial Z} = 0 \quad (6)$$

$$\frac{\partial Z_{pi}}{\partial X} = 0 \quad \frac{\partial Z_{pi}}{\partial Y} = 0 \quad \frac{\partial Z_{pi}}{\partial Z} = 1 \quad (7)$$

>From Equation 1, considering Equation 5, Equation 6 and Equation 7, the Equation 4 for the three translational variables leads to:

$$\frac{\partial f_i}{\partial X} = X_{pi} - X_{ai} \quad (8)$$

$$\frac{\partial f_i}{\partial Y} = Y_{pi} - Y_{ai} \quad (9)$$

$$\frac{\partial f_i}{\partial Z} = Z_{pi} - Z_{ai} \quad (10)$$

However for the three rotational output variables (φ, θ, ψ) more complex expressions will be generated. As these expressions have to be evaluated in each of the numerous postures comprising the discretized workspace, they must be optimized as much as possible, regarding the computational cost. Firstly, applying Equation 5, Equation 6 and Equation 7, the Equation 4 for orientation variables is transformed into:

$$\frac{\partial f_i}{\partial \varphi} = \frac{\partial f_i}{\partial X} \frac{\partial X_{pi}}{\partial \varphi} + \frac{\partial f_i}{\partial Y} \frac{\partial Y_{pi}}{\partial \varphi} + \frac{\partial f_i}{\partial Z} \frac{\partial Z_{pi}}{\partial \varphi} \quad (11)$$

$$\frac{\partial f_i}{\partial \theta} = \frac{\partial f_i}{\partial X} \frac{\partial X_{pi}}{\partial \theta} + \frac{\partial f_i}{\partial Y} \frac{\partial Y_{pi}}{\partial \theta} + \frac{\partial f_i}{\partial Z} \frac{\partial Z_{pi}}{\partial \theta} \quad (12)$$

$$\frac{\partial f_i}{\partial \psi} = \frac{\partial f_i}{\partial X} \frac{\partial X_{pi}}{\partial \psi} + \frac{\partial f_i}{\partial Y} \frac{\partial Y_{pi}}{\partial \psi} + \frac{\partial f_i}{\partial Z} \frac{\partial Z_{pi}}{\partial \psi} \quad (13)$$

In (Macho et al., 2009) are obtained the following expressions:

$$\frac{\partial X_{pi}}{\partial \varphi} = -(Y_{pi} - Y) \quad (14)$$

$$\frac{\partial Y_{pi}}{\partial \varphi} = X_{pi} - X \quad (15)$$

$$\frac{\partial Z_{pi}}{\partial \varphi} = 0 \quad (16)$$

$$\frac{\partial X_{pi}}{\partial \theta} = \cos \varphi (Z_{pi} - Z) \quad (17)$$

$$\frac{\partial Y_{pi}}{\partial \theta} = \sin \varphi (Z_{pi} - Z) \quad (18)$$

$$\frac{\partial Z_{pi}}{\partial \theta} = -\sin \varphi (Y_{pi} - Y) - \cos \varphi (X_{pi} - X) \quad (19)$$

$$\frac{\partial X_{pi}}{\partial \psi} = -\cos \theta (Y_{pi} - Y) + \sin \varphi \sin \theta (Z_{pi} - Z) \quad (20)$$

$$\frac{\partial Y_{pi}}{\partial \psi} = \cos \theta (X_{pi} - X) - \cos \varphi \sin \theta (Z_{pi} - Z) \quad (21)$$

$$\frac{\partial Z_{pi}}{\partial \psi} = \sin \theta [\cos \varphi (Y_{pi} - Y) - \sin \varphi (X_{pi} - X)] \quad (22)$$

4.3 IKP Jacobian

For fully-parallel manipulators, \mathbf{J}_{IKP} is diagonal. Each term of such diagonal is associated with one KC and it is given by the derivative of the characteristic equation f_i with respect to its input variable q_i . Therefore, $|\mathbf{J}_{IKP}|$ vanishes, producing an *IKP* singularity, whenever any of the diagonal terms does. This means that all KC can be considered independent sub-mechanisms capable of separately causing *IKP* singularities.

It would be useful if the values of different Jacobian terms were comparable among them. Thus, given a posture of the manipulator, which KC is closer to produce an *IKP* singularity could be determined. To do this a normalization of these terms has been implemented.

Instead of the actual value of the derivative $\partial f_i / \partial q_i$, another parameter, called normalized term of the \mathbf{J}_{IKP} , $\|\partial f_i / \partial q_i\|$, will be used. This parameter has a specific expression for each type of KC and its value is directly proportional to the corresponding term of the $|\mathbf{J}_{IKP}|$, and thus, vanishes at the *IKP* singular configuration of the KC. But its value is limited to 1 at the furthest position from the singularity. Next will be shown the expressions of $\|\partial f_i / \partial q_i\|$ for the KC comprising the manipulator under analysis:

- PSS KC:

$$\left\| \frac{\partial f_i}{\partial q_i} \right\| = \frac{(\mathbf{p}_i - \mathbf{a}_i) \cdot (\mathbf{f}_i - \mathbf{g}_i)}{R_i L_i} \quad (23)$$

- RSS KC:

$$\left\| \frac{\partial f_i}{\partial q_i} \right\| = \frac{[(\mathbf{a}_i - \mathbf{f}_i) \times \mathbf{e}_i] \cdot (\mathbf{p}_i - \mathbf{a}_i)}{R_i L_i} \quad (24)$$

IKP singularities occur whenever any *KC* reaches an extreme position, thus they define the workspace boundary. Taking this into account, it is easy to check all discrete postures added to the workspace in order to know which of them are closer to one of these singularities. If one posture is surrounded completely by neighboring positions in the discrete grid, it is inside the workspace, whereas if it lacks some neighbor it is in a border and hence it is an approximate *IKP* singularity.

Once one of these postures has been identified, comparing the values of the normalized elements corresponding to all *KC*, it is possible to know which *KC* has produced the singularity, that one with the smaller value. This result is depicted in Fig. 7-(b). This information will be necessary later on to plan working mode transitions in the enlarged operational workspace.

4.4 DKP singularity maps and workspace singularity-free regions

The mapping of $|J_{DKP}|$ on the workspace provides an approximate singularity map. In fact, the change in the sign of $|J_{DKP}|$ is the best way to detect a transition over a singular posture. This phenomenon has been used to obtain *DKP* singular postures within the computed workspace. Whenever two contiguous postures in the discrete grid with different signs are found, they are considered approximated singularities. Once all approximated singular postures are found, there is an easy way to refine the singular locus. Taking every two neighboring singular postures with opposite signs, by means of a linear interpolation that makes use of the actual values of the $|J_{DKP}|$, it can be placed an intermediate posture at the presumed null value of the determinant, as shown schematically in Fig. 8.

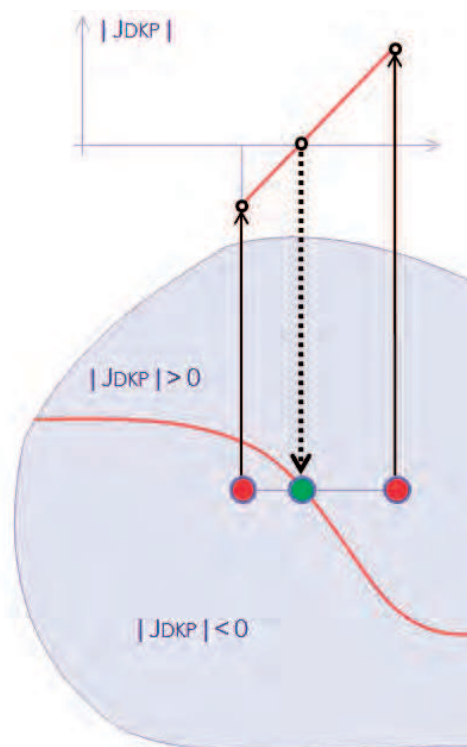


Fig. 8. *DKP* singularity refinement

DKP singularity locus divides the workspace into a set of regions free of internal singularities. For a three-dimensional workspace, like the one depicted in Fig. 7, the loci of postures

where the $|\mathbf{J}_{DKP}|$ vanishes defines a spatial surface which completely splits the aforementioned workspace into regions associated with different signs of such a kinematic indicator. These correspond with different assembly modes of the manipulator.

In \mathbf{J}_{DKP} appear the coordinates of nodes \mathbf{a}_i . For the same pose of the *MP*, the coordinates of such points are different for each *KC IKP* configuration. Therefore, each working mode of the manipulator has its own *DKP* singularity loci. This result is depicted in Fig. 9. The resulting workspace singularity-free regions associated to $|\mathbf{J}_{DKP}|$ positive and negative are the volumes depicted in Fig. 10.

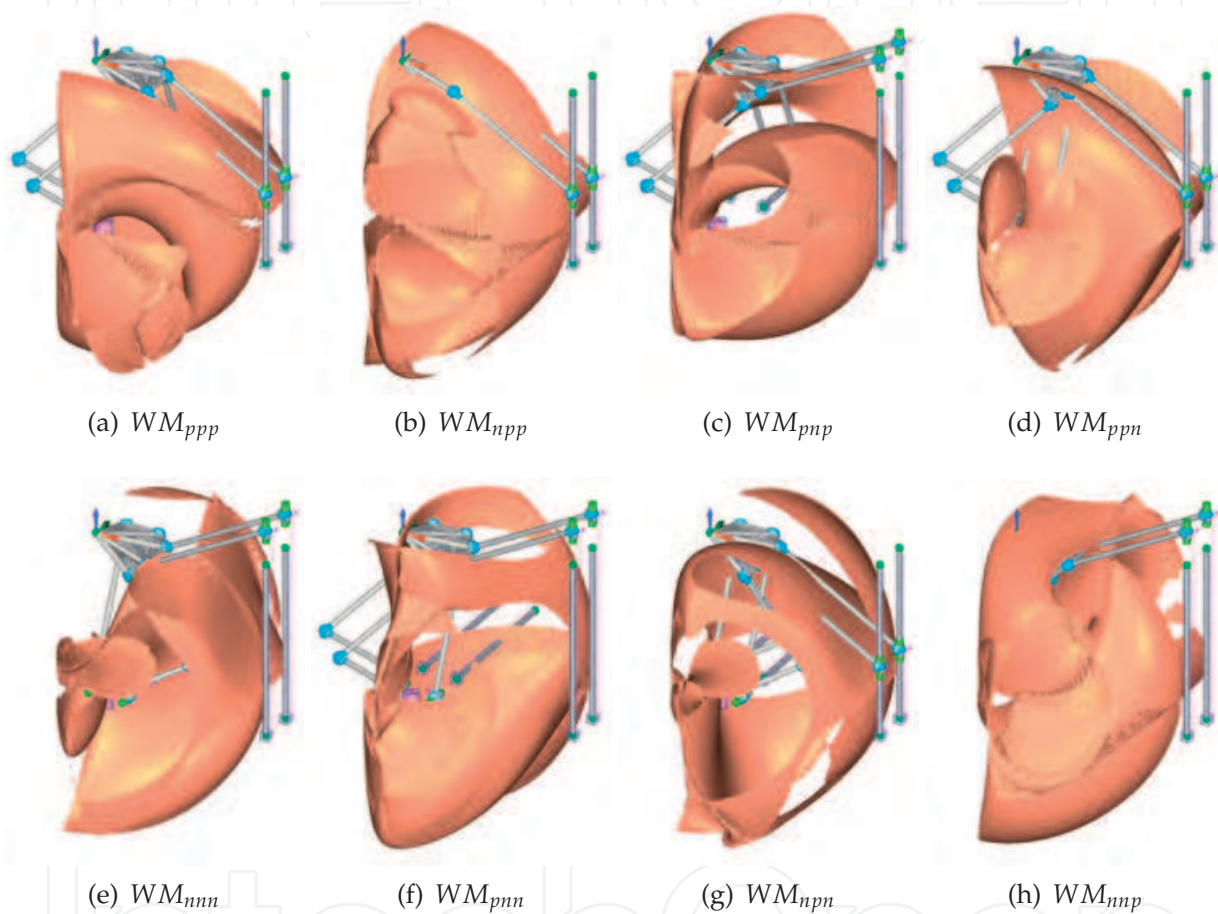


Fig. 9. *DKP* singularity surfaces for each working mode. Loci of postures with $|\mathbf{J}_{DKP}| = 0$

5. Enlarged operational workspace

As mentioned before, it is a common practice to define as the basic operational workspace one of these singularity-free regions, i.e., the region of the workspace associated with a working mode, in which the manipulator keeps the same assembly mode configuration. The robot will have its home posture in such a region and will be kept inside it all the time. However, it is also possible to consider the union of singularity-free regions associated with the same assembly mode. This requires a path planning implementing transitions between working modes, which will lead to an enlarged operational workspace.

Therefore, finally, there is a workspace, shown in Fig. 7, crossed by *DKP* singularities that must be avoided, shown in Fig. 9, which divide that workspace into a set of singularity-free

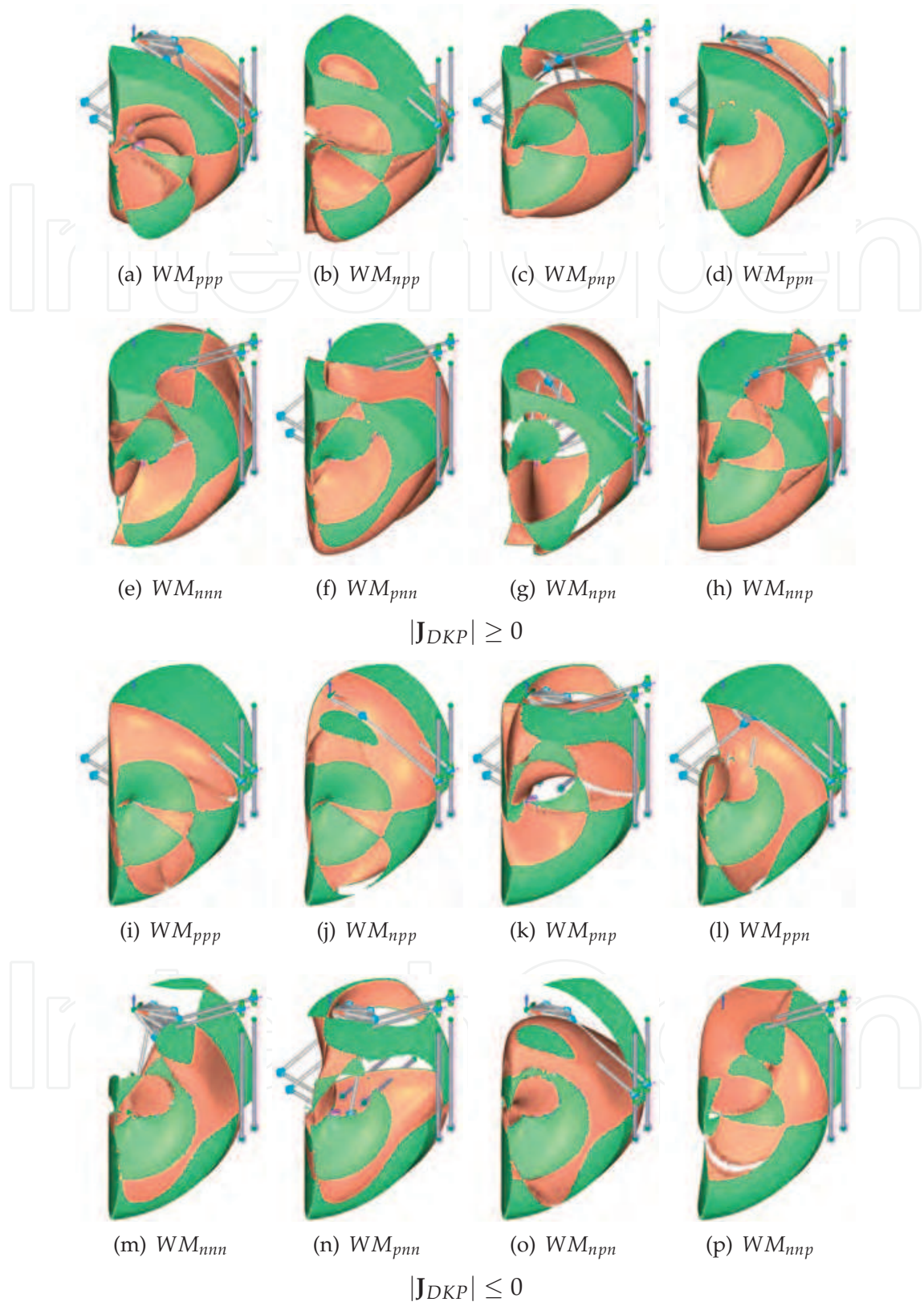


Fig. 10. Workspace singularity-free regions

regions, Fig. 10, that are obviously smaller than the complete workspace. Alternatively, the enlarged operational workspace associated with an assembly mode, also being usually smaller than the total workspace, since comes from the union of several singularity-free regions, is normally larger than any of such composing regions, and thus, can be defined as the largest set of postures that the manipulator can reach without the blockade of the actuators.

The analysis of the operational workspace done in the obtained three-dimensional workspace may result confusing. In order to understand these concepts clearly, only a plane section of the workspace will be considered. A bi-dimensional analysis will be much more illustrative and the explained ideas can be immediately extrapolated to the three-dimensional entity. Remember that according to the procedure described, just the desired output variables are incremented in the discrete grid. So, configuring the workspace computation grid only in variables (Y, Z) , a planar slice, for a constant value of the output variable $X = 0$, of the whole workspace will be obtained, as shown in Fig. 11.

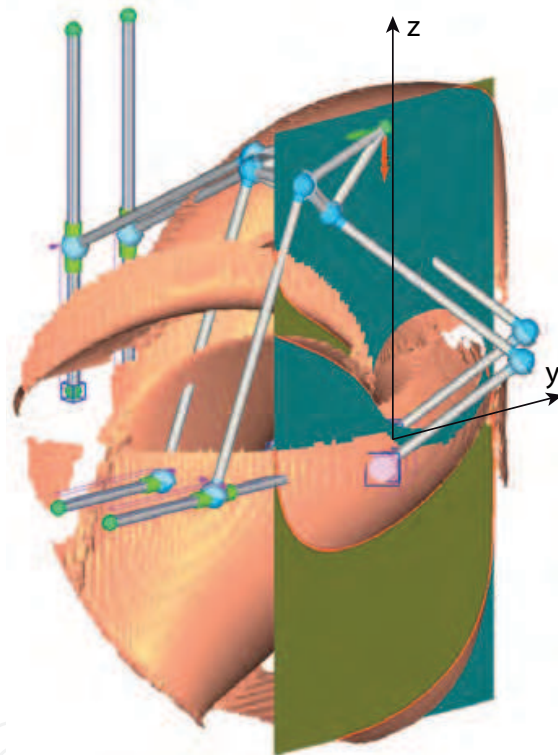


Fig. 11. Planar slice of the workspace for a constant value of X

Thus, without losing generality, it will be assumed that the robot moves in such a way that the *TCP* is always on that plane. In this planar case, singularity loci are defined by curves. As shown in Fig. 11, the singularity curves in the bidimensional case are the intersections between the considered plane and the general three-dimensional singularity surfaces. In Fig. 12 are shown the workspace singularity-free regions associated with different signs of $|\mathbf{J}_{DKP}|$ for the eight existing working modes.

The enlarged, or maximal, operational workspace associated to an assembly mode will be obtained overlapping the singularity-free regions, corresponding to all existing working modes, associated with that assembly mode. This result is shown in Fig. 13. As it can be observed, obtained enlarged operational workspaces do not fill completely the complete workspace, but the not reachable areas are just quite small corners (less than a 5% of the whole surface).

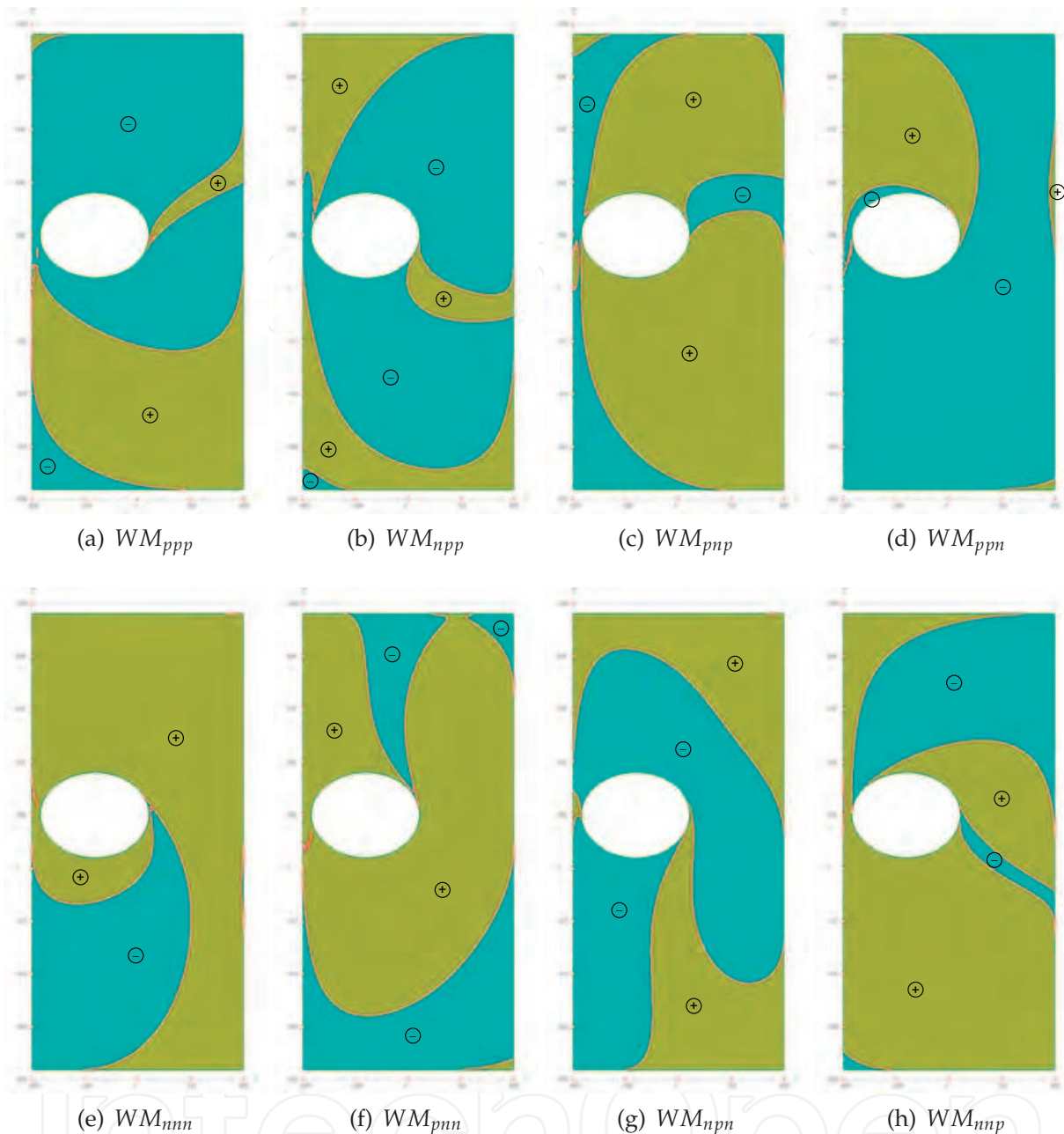


Fig. 12. Workspace singularity-free regions in a bi-dimensional section

5.1 Path planning inside the maximal operational workspace

After having obtained the singularity-free regions of the workspace associated with all working and assembly modes, the strategies to enlarge the accessible space are easier to plan and implement. To do this, it is necessary to know and use, as said before, *IKP* singularities, because they enable transitions between regions associated to different working modes. By virtue of this knowledge, appropriate paths can be defined to fulfill with desired motion planning tasks.

As an example let's suppose that the manipulator is initially configured in the WM_{ppp} working mode, with the *TCP* located in the initial position, p_i , shown in Fig. 14-(a). This posture

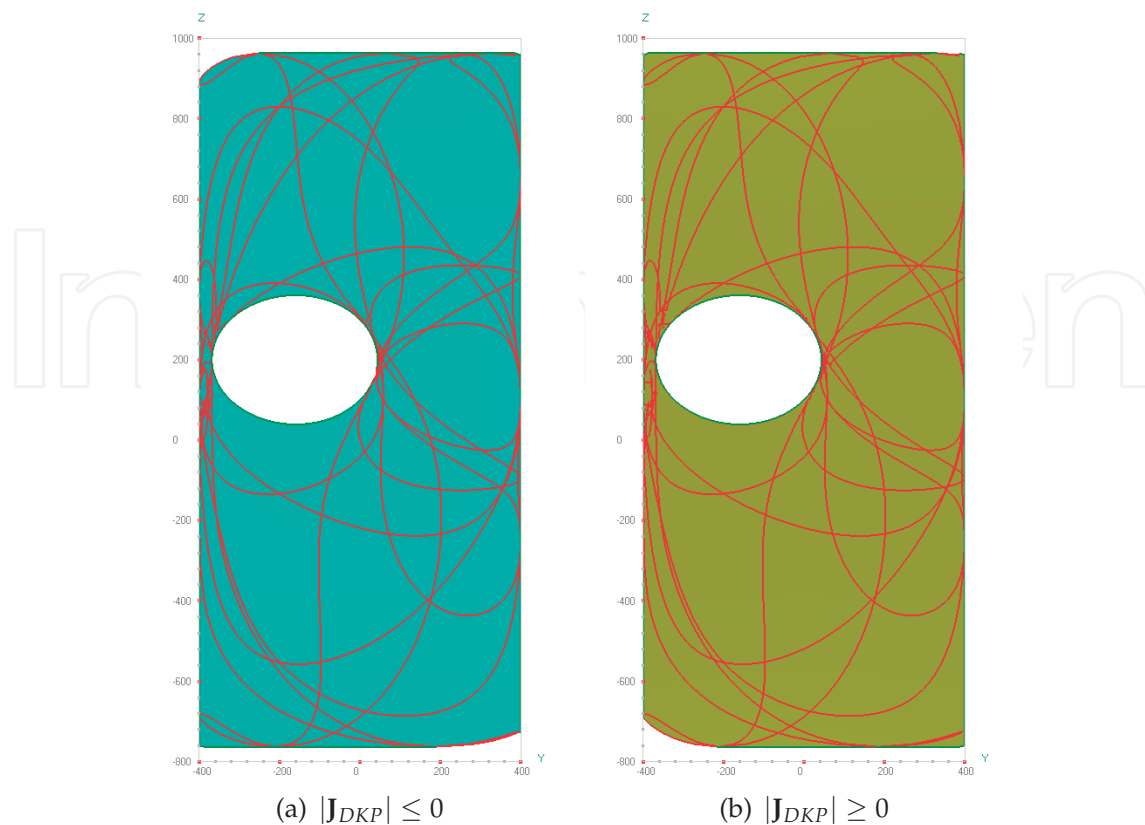


Fig. 13. Maximal operational workspaces associated with existing assembly modes. Superimposition of all singularity-free regions associated with the same sign of $|\mathbf{J}_{DKP}|$

is located in a singularity-free region associated with $|\mathbf{J}_{DKP}| \leq 0$ assembly mode. According to this, in Fig. 14-(b) all regions associated with $|\mathbf{J}_{DKP}| \geq 0$ have been removed. But the remaining workspace is still composed by several disjoint singularity-free regions, all of them associated with $|\mathbf{J}_{DKP}| \leq 0$. Although all of them have been initially considered as belonging to the same assembly mode, the current elemental operational workspace is given by the the region that contains the *TCP* location, i.e., that one depicted in Fig. 14-(c).

>From this initial region, on reaching the *IKP* singularity curve highlighted with a dashed line in Fig. 15-(a), the KC_3 in Fig. 1 can change its *IKP* configuration. Thus, the manipulator will change its working mode from WM_{ppp} to WM_{ppn} . At that moment *DKP* singularity curves, which are specific for each working mode, change and the workspace becomes divided into new singularity-free regions. The new region where the robot can move without losing control is depicted in Fig. 15-(b). The transition from one region to another is performed always via the *IKP* singularity locus due to the *KC* that changes its configuration. In fact those curves (surfaces in the case of the general three-dimensional workspace) are completely shared by the regions connected, as shown in Fig. 15-(c). Once the new region has been reached, new postures in the workspace are attainable, for example p_f in Fig. 15-(b). Also some postures that were attainable in the starting region cannot be directly reached now, like p_i .

The overlapping of the two regions corresponding to WM_{ppp} and WM_{ppn} working modes, Fig. 15-(c), almost fill the enlarged operational workspace corresponding to $|\mathbf{J}_{DKP}| \leq 0$, indicated in Fig. 13-(a). But lacking postures can be reached making another working mode

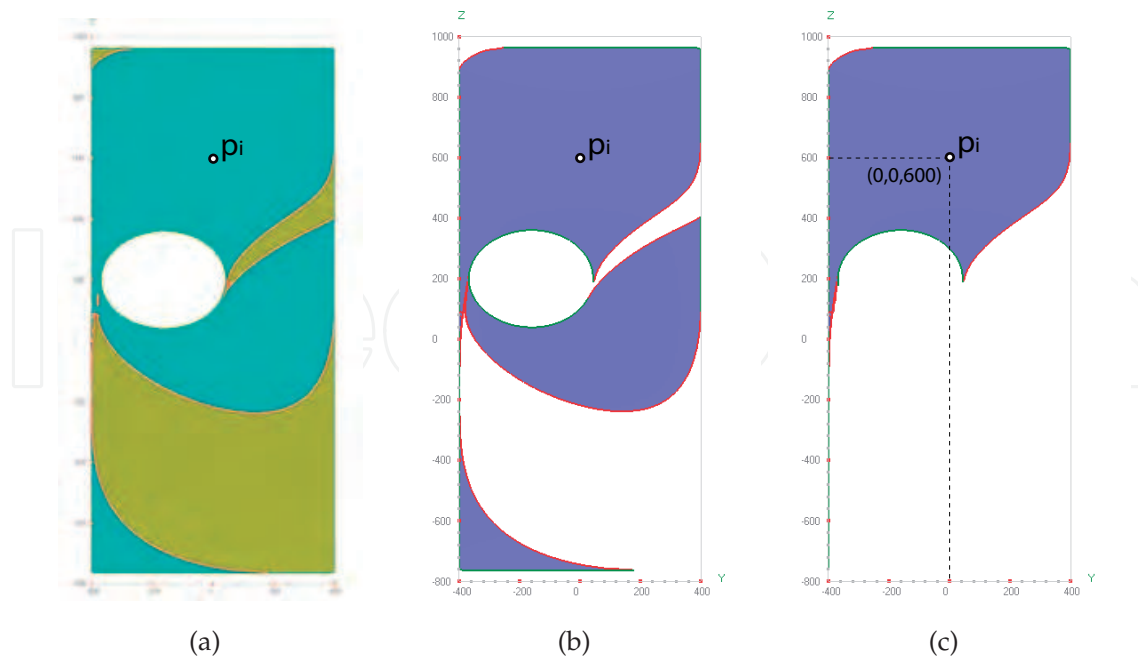


Fig. 14. Initial posture and corresponding singularity-free region

change since they are inside the region corresponding to the WM_{npp} working mode. Thus, starting from the same initial region, associated with the WM_{ppp} working mode, on reaching a posture over the IKP singularity curve highlighted with dashed line in Fig. 15-(d), the KC_1 will change its configuration form p to n to perform the desired transition between working modes. Doing this, the region depicted in Fig. 15-(e) is reached, enlarging the initial operational workspace as shown in Fig. 15-(f).

In this example, just overlapping three singularity-free regions, those corresponding to WM_{ppp} , WM_{ppn} and WM_{npp} working modes, the maximal enlarged operational workspace associated with $|J_{DKP}| \leq 0$ is fulfilled. Nevertheless, additional transitions connecting all other working mode regions are feasible. In Fig. 16 are shown all the possibilities starting from the initial region depicted in Fig. 14-(c). Next to the connection lines displayed is indicated which KC changes its configuration to make the transition between connected regions. Note that there are some regions in Fig. 16 which cannot be reached (not colored regions) and some working mode changes that are not possible (dashed connection lines) because the corresponding initial and final regions do not share the adequate IKP singularity curve.

In consequence, operational workspace enlargement capability may depend on the region where the manipulator is initially configured. For example, if the starting region was the one marked in Fig. 18, only the color filled regions will be accessible, resulting on an operational workspace, shown in Fig. 19 smaller than the one achieved in Fig. 17. This fact has to be taken into account when making the path planning.

A transition scheme, like the one shown in Fig. 16, is very useful to perform the path planning task. For example, let's suppose that the manipulator has to from the initial posture p_i , to the final posture p_f shown in Fig. 20-(a). Let's suppose also that the manipulator will work according to the $|J_{DKP}| \leq 0$ assembly mode. Since both postures belong to the enlarged operational workspace, it is known in advance that the robot will be able to join them in a controlled way. And finally, let's suppose that there are some technical hypothetical rea-

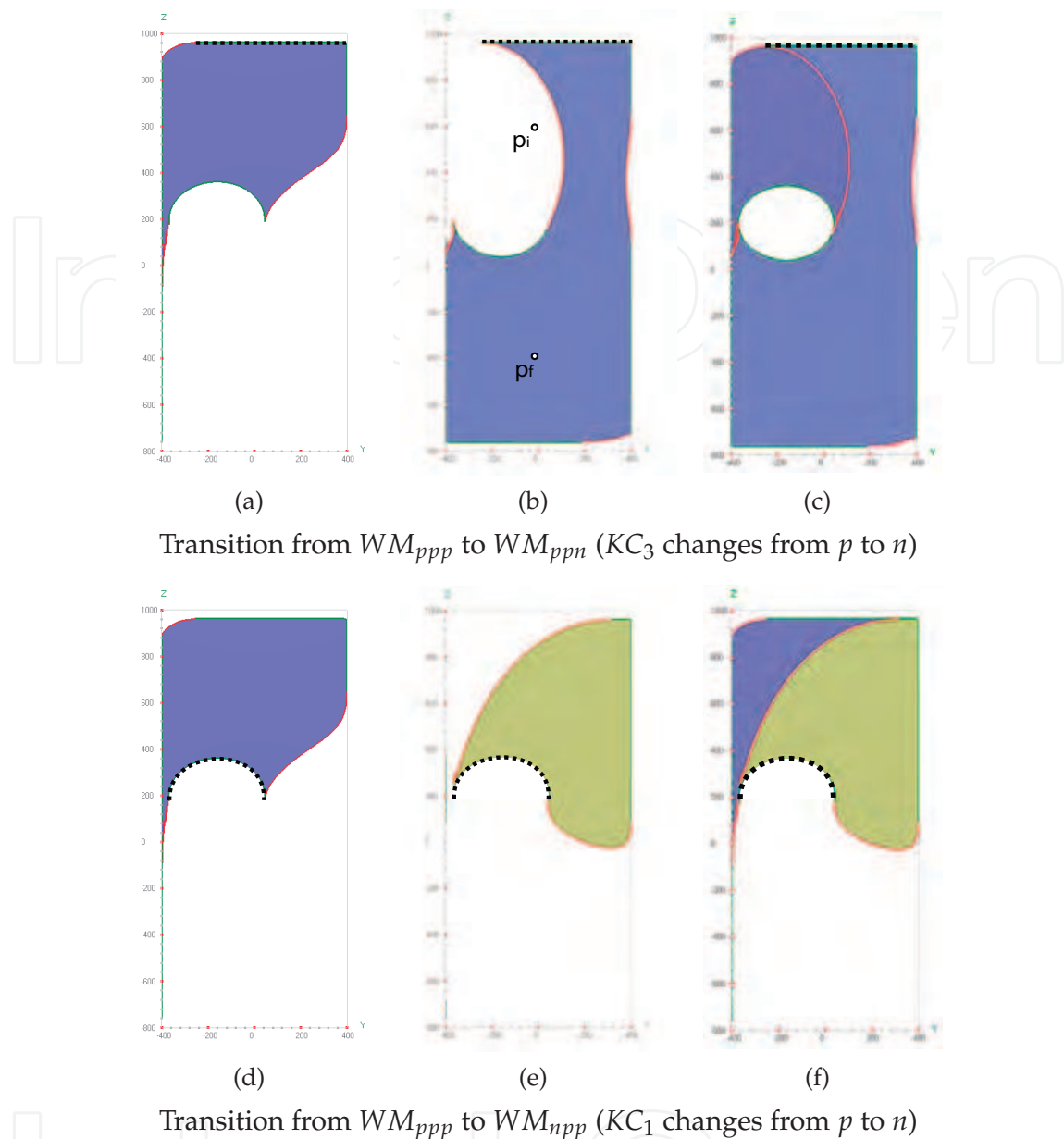


Fig. 15. Transitions between singularity-free regions through *IKP* singularities

sons which impose that the the manipulator must start in the initial posture configured in the WM_{ppp} working mode and must reach the final posture configured in the WM_{nnn} working mode. In Fig. 20-(b) and (c) are shown the initial and final singularity-free regions, containing the initial and final postures, which must be joined making working mode changes.

The map in Fig. 16 allows to know easily how to go from p_i to p_f verifying also the prescribed initial and final working modes. Note that as the three KC have to change their configuration, at least three transitions will be required. There are several possibilities, or ways, for joining the initial and final regions. Just one will be depicted in Fig. 21:

- Starting from the initial position p_i in the WM_{ppp} working mode, the *TCP* of the manipulator goes to the intermediate position p_{g1} over the *IKP* singularity curve caused by KC_3 to make transition to the WM_{ppn} working mode, Fig. 21-(a).

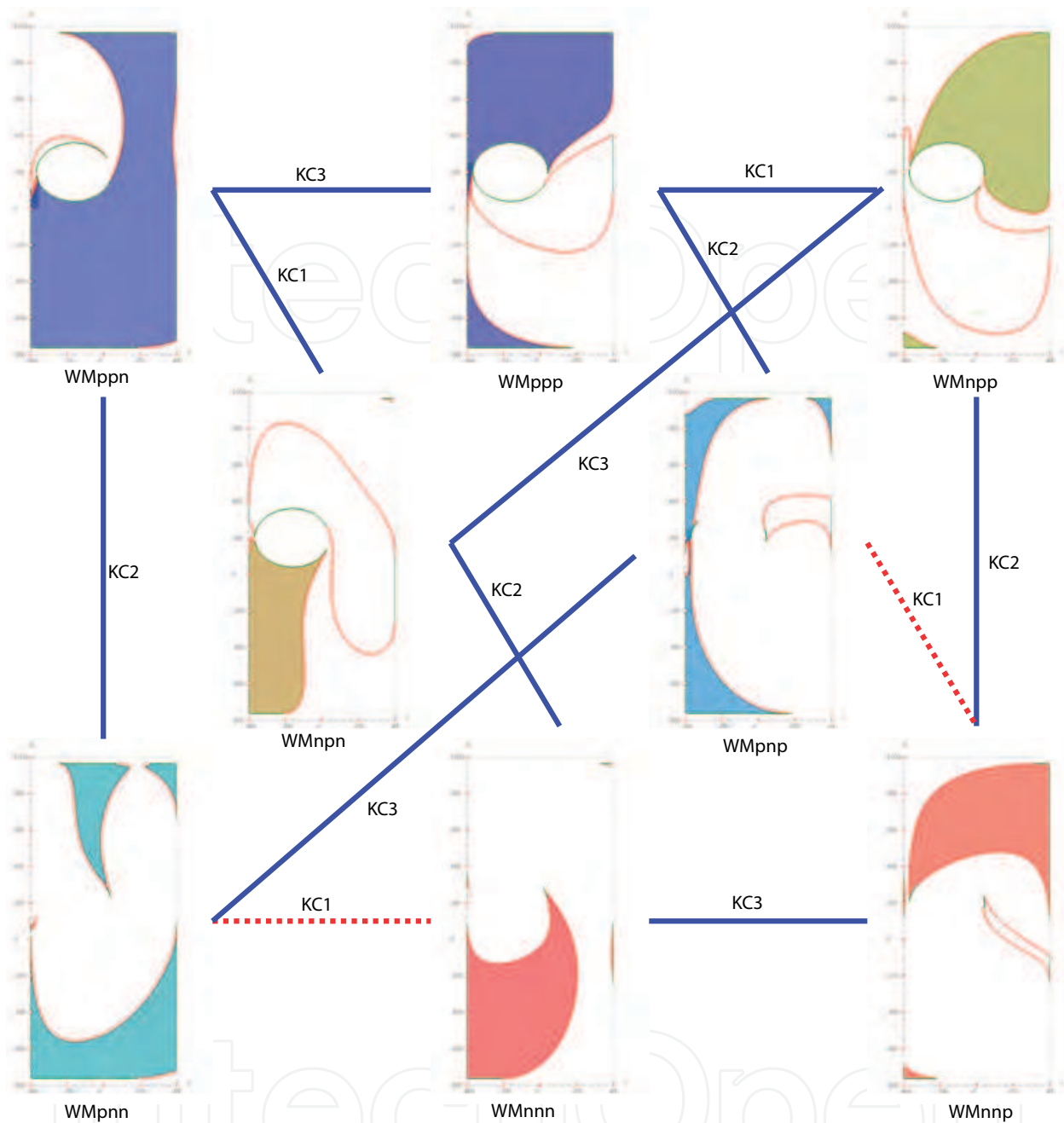


Fig. 16. Transitions among singularity-free regions associated with different working modes

- On reaching the new region, the motion has to continue inside it from p_{g1} , to the second intermediate position p_{g2} over the *IKP* singularity curve caused by KC_2 to make transition to the WM_{pnn} working mode, Fig. 21-(b).
- On reaching the third region, the motion has to continue inside it from p_{g2} , to the third intermediate position p_{g3} over the *IKP* singularity curve caused by KC_1 to make transition to the WM_{nnp} working mode, Fig. 21-(c).
- Finally, the motion can evolve inside the final region to the final posture p_f , Fig. 21-(d).

All motions have been done without reaching any *DKP* singularity.

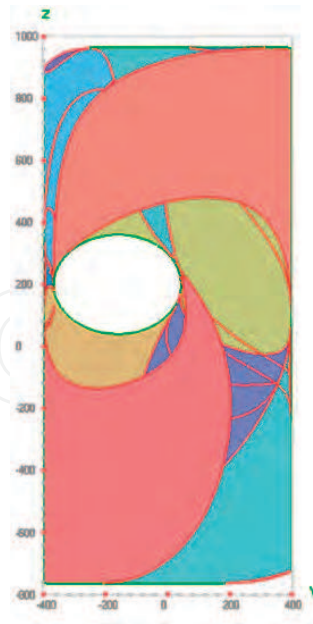


Fig. 17. Overlapping of all joined singularity-free regions. Enlarged operational workspace

Generalizing the described process, to go from a singularity-free region associated with a working mode $WM_{i,j,\dots,k}$, to another region associated with $WM_{l,m,\dots,n}$, they must be done consecutively as many elemental transitions as kinematic chains have to change their configuration, namely:

- from $WM_{i,j,\dots,k}$ to $WM_{l,j,\dots,k}$
- from $WM_{l,j,\dots,k}$ to $WM_{l,m,\dots,k}$
- ...
- from $WM_{l,m,\dots,k}$ to $WM_{l,m,\dots,n}$

This way any pose inside the operational workspace can be reached without blockade of actuators. All these procedures can be generalized directly to the complete three-dimensional workspace. In Fig. 22 are shown the enlarged operational workspaces associated with the two existing assembly modes. A size comparison (in volume) among the complete workspace, Fig. 7, the largest singularity-free region (WM_{npp} , Fig. 10-(o)) and the enlarged operational workspace associated with the assembly mode $|J_{DKP}| \leq 0$, Fig. 22-(b) can be done resulting on:

- Complete workspace: 100%
- Largest singularity-free region: 75%
- Enlarged operational workspace: 97%

6. Conclusions

This chapter has described and illustrated the strategy of obtaining enlarged workspaces connecting all working modes and keeping one of the parallel manipulator assembly modes. It has been used a procedure which is able to obtain all the singularity-free regions of the

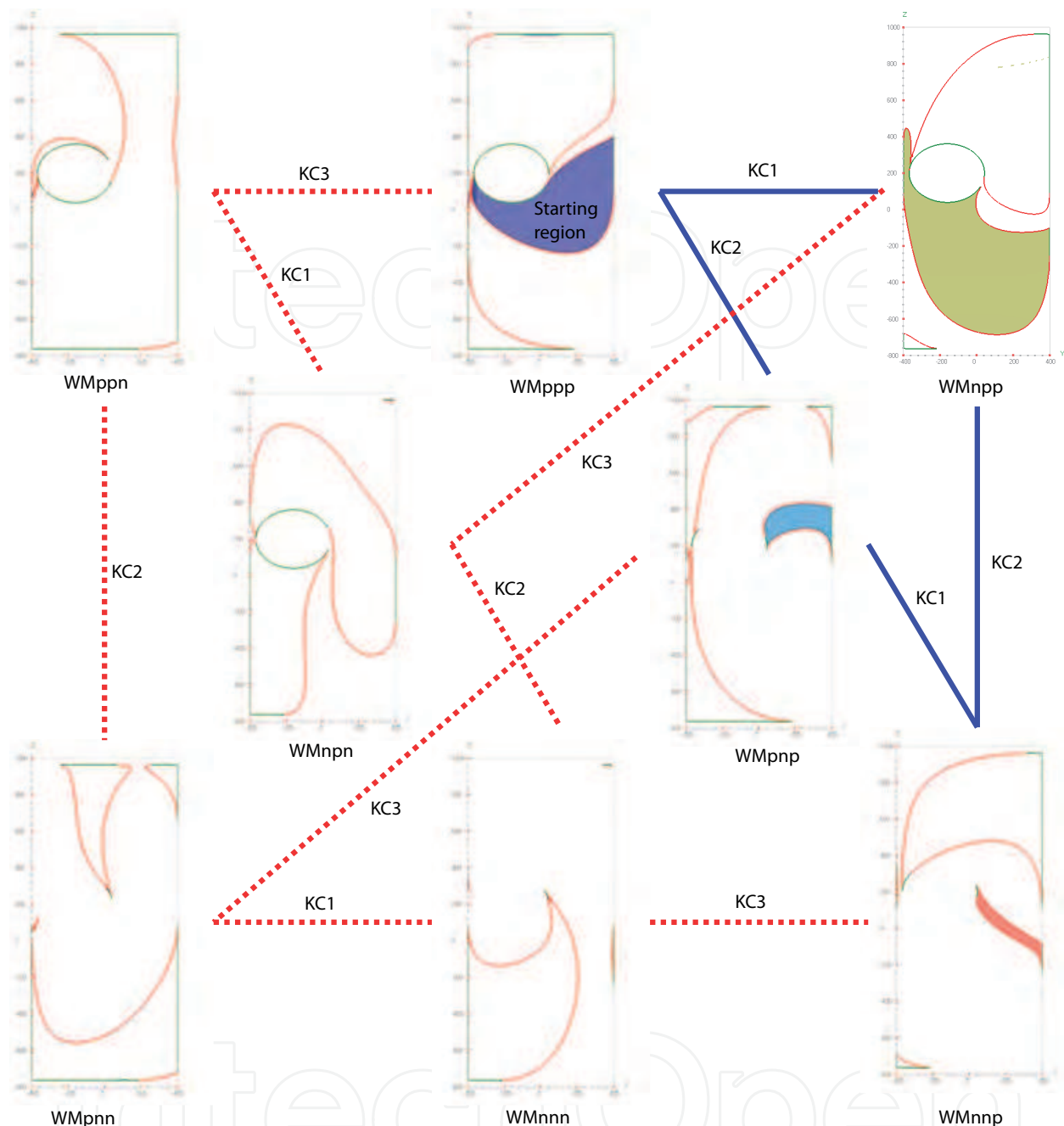


Fig. 18. Feasible transitions starting from another region

robot workspace, taking into account that each working mode presents a different direct kinematic problem singularity locus. The direct singularities imply that a dependency relation appears among actuator velocities and separate assembly modes, while the inverse singularities, which define the workspace boundaries and separate working modes, can be reached without loss of control. Therefore, it is possible to make use of the inverse singularities to transit between different singularity-free regions associated with the same assembly mode. Joining all the regions associated with the same assembly mode for all working modes, the largest set of postures that the manipulator can reach is obtained. In order to make an efficient path planning within this enlarged workspace, the workspace borders allowing the transi-

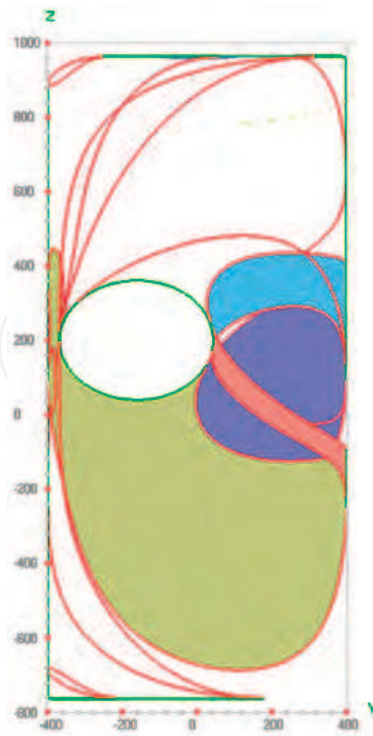


Fig. 19. Joined singularity-free regions. Enlarged operational workspace starting from another region

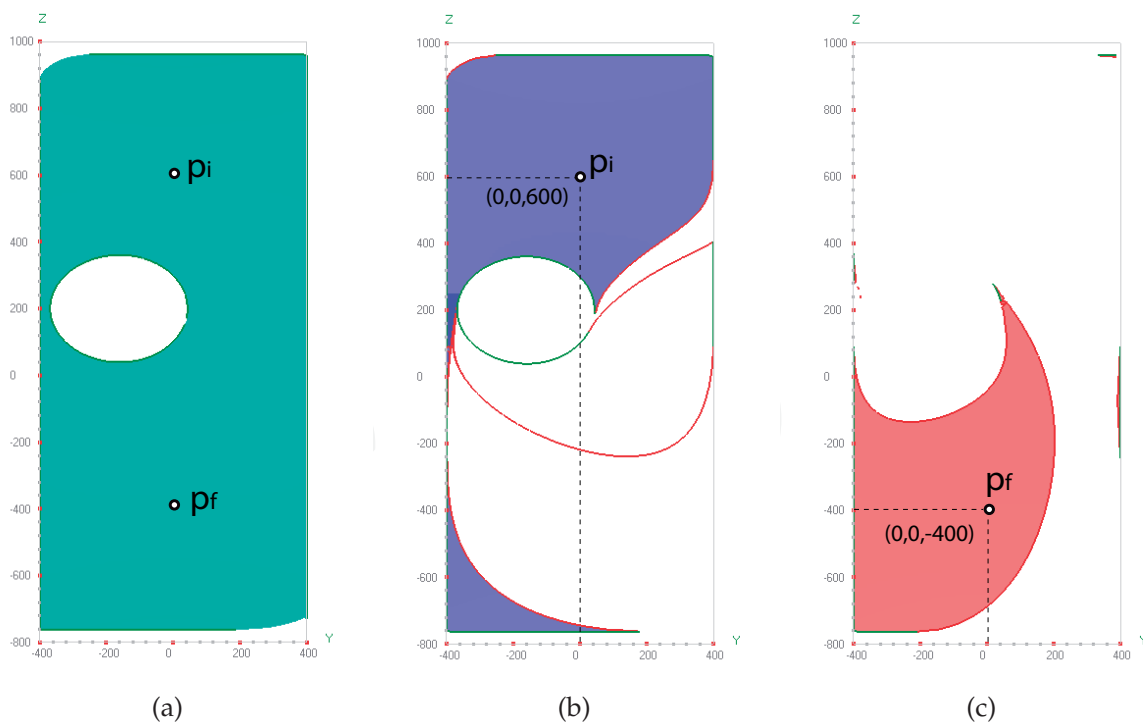


Fig. 20. Initial and final postures in the enlarged operational workspace and in their singularity-free regions

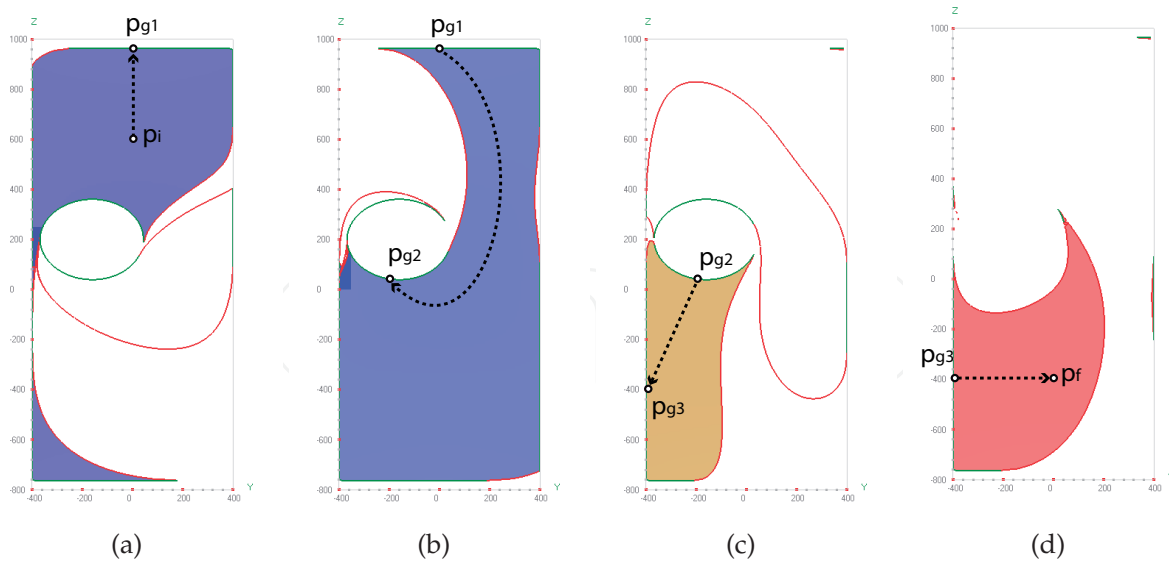


Fig. 21. Path planning

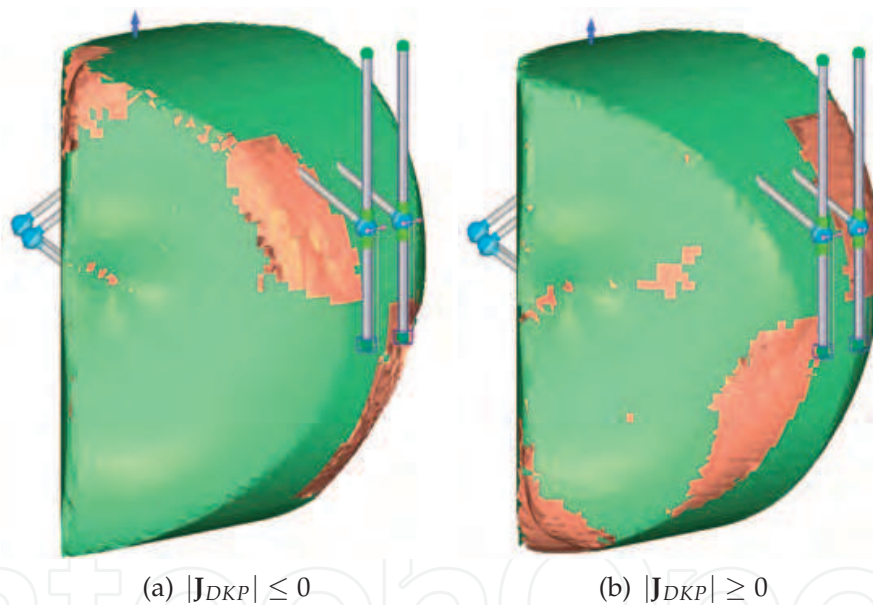


Fig. 22. Enlarged three-dimensional workspace

tions between the different working modes need to be known and used. This is the first time that the systematic general purpose procedure has been applied to a *Delta like* manipulator by means of an auxiliary equivalent robot.

Acknowledgment

This research work was supported in part by the Spanish Ministerio de Ciencia y Tecnología (Project DPI2008-00159), the FEDER funds of the European Union, the University of the Basque Country (Project GIU07/78) and the Grant (BFI104.148.R2) from the Basque Government.

7. References

- Agrawal, S. (1991). Workspace boundaries of in-parallel manipulator systems, *IEEE Journal on Robotics and Automation* **7(2)**: 94–99.
- Altuzarra, O., Pinto, C., Aviles, R. & Hernandez, A. (2004). A practical procedure to analyze singular configurations in closed kinematic chains, *IEEE Transactions on Robotics* **20(6)**: 929–940.
- Bonev, I. & Ryu, J. (1999). Workspace analysis of 6-prrs parallel manipulators based on the vertex space concept, *ASME Design Engineering Technical Conference*.
- Dash, A., Yeo, S., Yang, G. & Chen, I. (2002). Workspace analysis and singularity representation of three-legged parallel manipulators, *ICARCV 02* pp. 962–967.
- Gosselin, C. (1990). Determination of workspace of 6-dof parallel manipulators, *ASME Journal of Mechanical Design* **112**: 331–336.
- Gosselin, C. & Angeles, J. (1990). Singularity analysis of closed loop kinematic chains, *IEEE Transactions on Robotics and Automation* **6(3)**: 281–290.
- Gregorio, R. D. (2004). Determination of singularities in delta-like manipulators, *The International Journal of Robotics Research* **23(1)**: 89–96.
- Hunt, K. & Primrose, E. (1993). Assembly configurations of some in-parallel-actuated manipulators, *Mechanism and Machine Theory* **28(1)**: 31–42.
- Innocenti, C. & Parenti-Castelli, V. (1992). Singularity free evolution from one configuration to another in serial and fully parallel manipulators, *ASME Journal of Mechanical Design* **120**: 73–99.
- Jo, D. & Haug, E. (1998). Workspace analysis of closed-loop mechanisms with unilateral constraints, *ASME Design Automation Conference* pp. 53–60.
- Laribi, M., Romdhane, L. & Zeghloul, S. (2007). Analysis and dimensional synthesis of the delta robot for a prescribed workspace, *Mechanism and Machine Theory* **42**: 859–870.
- Li, H., Gosselin, C. & Richard, M. (2007). Determination of the maximal singularity-free zones in the six-dimensional workspace of the general gough–Stewart platform, *Mechanism and Machine Theory* **42(4)**: 497–511.
- Liu, X., Wang, J., Oh, K. & Kim, J. (2004). A new approach to the design of a delta robot with a desired workspace, *Journal of Intelligent and Robotic Systems* **39**: 209–225.
- Lopez, M., Castillo, E., Garcia, G. & Bashir, A. (2005). Delta robot: inverse, direct, and intermediate jacobians.
- Macho, E., Altuzarra, O., Amezua, E. & Hernandez, A. (2009). Obtaining configuration space and singularity maps for parallel manipulators, *Mechanism and Machine Theory* **44(11)**: 2110–2125.
- Macho, E., Altuzarra, O., Pinto, C. & Hernandez, A. (2008a). Transitions between solutions of the direct kinematic problem, *Advances in Robot Kinematics*.
- Macho, E., Altuzarra, O., Pinto, C. & Hernandez, A. (2008b). Workspaces associated to assembly modes of the 5r planar parallel manipulator, *Robotica* **26(3)**: 395–403.
- Masory, O. & Wang, J. (1995). Workspace evaluation of stewart platforms, *Advanced Robotics* **9(4)**: 443–46.
- McAree, P. & Daniel, R. (1999). An explanation of the never-spacial assembly changing motions for 3-3 parallel manipulators, *The International Journal of Robotics Research* **18(6)**: 556–574.
- Merlet, J., Gosselin, C. & Mouly, N. (1998). Workspace of planar parallel manipulators, *Mechanism and Machine Theory* **33(1-2)**: 7–20.



Robot Manipulators New Achievements

Edited by Aleksandar Lazinica and Hiroyuki Kawai

ISBN 978-953-307-090-2

Hard cover, 718 pages

Publisher InTech

Published online 01, April, 2010

Published in print edition April, 2010

Robot manipulators are developing more in the direction of industrial robots than of human workers. Recently, the applications of robot manipulators are spreading their focus, for example Da Vinci as a medical robot, ASIMO as a humanoid robot and so on. There are many research topics within the field of robot manipulators, e.g. motion planning, cooperation with a human, and fusion with external sensors like vision, haptic and force, etc. Moreover, these include both technical problems in the industry and theoretical problems in the academic fields. This book is a collection of papers presenting the latest research issues from around the world.

How to reference

In order to correctly reference this scholarly work, feel free to copy and paste the following:

E. Macho, O. Altuzarra and A. Hernandez (2010). Maximal Operational Workspace of Parallel Manipulators, Robot Manipulators New Achievements, Aleksandar Lazinica and Hiroyuki Kawai (Ed.), ISBN: 978-953-307-090-2, InTech, Available from: <http://www.intechopen.com/books/robot-manipulators-new-achievements/maximal-operational-workspace-of-parallel-manipulators>

INTECH
open science | open minds

InTech Europe

University Campus STeP Ri
Slavka Krautzeka 83/A
51000 Rijeka, Croatia
Phone: +385 (51) 770 447
Fax: +385 (51) 686 166
www.intechopen.com

InTech China

Unit 405, Office Block, Hotel Equatorial Shanghai
No.65, Yan An Road (West), Shanghai, 200040, China
中国上海市延安西路65号上海国际贵都大饭店办公楼405单元
Phone: +86-21-62489820
Fax: +86-21-62489821

© 2010 The Author(s). Licensee IntechOpen. This chapter is distributed under the terms of the [Creative Commons Attribution-NonCommercial-ShareAlike-3.0 License](#), which permits use, distribution and reproduction for non-commercial purposes, provided the original is properly cited and derivative works building on this content are distributed under the same license.

IntechOpen

IntechOpen